



Experimental investigation on the nanoindentation viscoelastic constitutive model of quartz and kaolinite in mudstone

Changlun Sun¹ · Guichen Li¹ · Mohamed Elgharib Gomah^{1,2} · Jiahui Xu¹ · Haoyu Rong¹

Received: 1 June 2020 / Revised: 16 July 2020 / Accepted: 14 December 2020 / Published online: 9 February 2021
© The Author(s) 2021

Abstract The creep behaviors in deep underground engineering structures, especially in soft rocks, have a remarkable impact on the long-term stability of the excavations, which finally leads to the high risk and failure of it. Accordingly, it is essential to recognize the time-dependent deformation through the investigation of this phenomenon. In this study, the creep behaviors of soft rocks were examined to help understand the underlying mechanism of the extended time-dependent deformation. Due to the limited results about the time-dependent properties of the constituents of the rock that reveal their heterogeneity, the targeting nanoindentation technique (TNIT), was adopted to investigate the viscoelastic characteristics of kaolinite and quartz in a two-constituent mudstone sample. The TNIT consists of identifications of mineralogical ingredients in mudstone and nanoindentation experiments on each identified constituent. After conducting experiments, the unloading stages of the typical indentation curves were analyzed to calculate the hardness and elastic modulus of both elements in mudstone. Additionally, the 180 s load-holding stages with the peak load of 50 mN were transformed into the typical creep strain–time curves for fitting analysis by using the Kelvin model, the standard viscoelastic model, and the extended viscoelastic model. Fitting results show that the standard viscoelastic model not only can perfectly express the nanoindentation creep behaviors of both kaolinite and quartz but also can produce suitable constants used to measure their creep parameters. The creep parameters of kaolinite are much smaller than that of quartz, which causes the considerable time-dependent deformation of the soft mudstone. Eventually, the standard viscoelastic model was also verified on the quartz in a sandstone sample.

Keywords Mudstone · Constituents · Viscoelastic properties · TNIT · Creep constitutive model

1 Introduction

Creep property, a time-dependent behaviour, is the inherent attributes of rocks, soft mudstone in particular (Sun 2007). In deep underground engineering, the creep deformations of rocks become more common due to the high stress (He

et al. 2005). The time-dependent deformations of rocks negatively affect the mining safety (Li et al. 2017; Mishra and Verrna 2015; Sainoki and Mitri 2017; Zhou et al. 2019), backfill mining (Guo et al. 2019; Sun et al. 2013), coalbed methane production (Danesh et al. 2016, 2017; Guo et al. 2018; Kang et al. 2015), and geo-sequestration (Liu et al. 2015; Sone and Zoback 2014). Consequently, to enhance the understanding of this phenomenon is of importance to guarantee the stability of underground engineering. Macro-scale laboratory creep experimental methods, such as uniaxial and triaxial compression tests, have been broadly used to investigate the rheological deformations of rocks which threw light on their creep characteristics (Sha et al. 2018; Xiong et al. 2019; Yang et al. 2015a, b). However, these experiments were too

✉ Guichen Li
liguichen@cumt.edu.cn

¹ School of Mines, Key Laboratory of Deep Coal Resource Mining, Ministry of Education of China, China University of Mining and Technology, Xuzhou 221116, Jiangsu, China

² Mining and Petroleum Engineering Department, Faculty of Engineering, Al-Azhar University, Cairo 11435, Egypt

complicated. On the one hand, the load-holding time of some triaxial compressive tests was about several days (Sone and Zoback 2014; Xu et al. 2014) and that for uniaxial compression tests was above 6 h (Jia et al. 2018; Yang et al. 2015a, b). On the other hand, the specimens used in macro-scale laboratory creep tests needed to meet strict size requirements: the typical cylindrical specimen size was $\Phi 50 \text{ mm} \times 100 \text{ mm}$ (Mishra and Verrna 2015) and the size of the smaller prismatic samples was $25 \text{ mm} \times 25 \text{ mm} \times 50 \text{ mm}$ (Lu and Wang 2017). Besides, centimetre-scale laboratory experiments regard rocks consisting of various constituents (Guery et al. 2008) as homogeneous bodies, where the underlying mechanism of large creep deformation of soft mudstone yet remains to be relatively insufficiently understood. Adopting a new technique to identify various mineralogical constituents and investigate their creep characteristics is very meaningful since the individual behaviour of each constituent dictates the overall behaviour of macro-scale mudstone.

Nanoindentation technique, also called the depth-sensing indentation, was first proposed and used by Kalei in 1968 in Russia (Kalei 1968). This technique has proven to be an effective and convenient method for determining the elastoplastic mechanical properties of solids based on a small rock sample, most notably elastic modulus, hardness (Oliver and Pharr 1992) and fracture toughness (Zeng et al. 2019). Merged with CT (Zhang et al. 2018a, b, c), SEM-EDS (Slim et al. 2019; Sun et al. 2020a, b), XRD (Zhao et al. 2019), and 3D printing (Kong et al. 2019) observing the microstructures of rock samples, nanoindentation technique was useful to investigate the mechanical behaviors of mineralogical components of shale, granite, coal or mudstone samples. The influence of clay minerals and kerogen on both the hardness and elastic modulus of organic-rich and clay-bearing shale was investigated (Abedi et al. 2016; Alstadt et al. 2015). Zhang Fan et al. obtained the hardness and elastic modulus of compositions in granite (Fan et al. 2017). Taking Chinese sub-bituminous coal as an example, the relationship between its morphologies and its nano-mechanical properties was investigated (Zhang et al. 2018a, b, c); Meng et al. and Sun et al. calculated the mean values of the nanoindentation mechanical parameters to represent that of standard coal samples (Meng et al. 2020; Sun et al. 2020a, b) and discussed the influence of quartz and kaolinite on the mechanical properties of coal matrix (Sun et al. 2020a, b). For mudstone samples, the nanoindentation technique can test the elastic and plastic mechanics of its minerals (Magenet et al. 2011) and reveal its heterogeneity (Auvray et al. 2017; Zhang et al. 2018a, b, c). However, all geomaterials also exhibit a viscoelastic response, which has encouraged researchers to improve the utilization of this technique on capturing and modelling the creep

characteristics of geomaterials. Slim et al. covered the role of the organic matter on creep rates of gas shale by using the nanoindentation technique and obtained that organic matter drives its creep rates (Slim et al. 2019). Liu et al. used nanoindentation technique to examine the creep behaviour of multi-phase oil shale by applying Burgers models and the logarithmic function to quantify creep curves of various phases in oil shale (Liu et al. 2017, 2018). Nevertheless, rock creep was usually observed as an increase in depth during the load-holding period at maximum load (Slim et al. 2019), and there is no work on how the creep strain–time data can be used to model the nanoindentation creep response. Besides, widely used grid nanoindentation method with hundreds of indentations (Liu et al. 2017, 2018) complicate the data analysis.

In this context, the nanoindentation technique coupled with XRD, SEM, and EDS, were used to inspect the creep behaviours of mineralogical constituents in mudstone. This paper is structured as follows: The studied two-constituent mudstone was first presented together with the nanoindentation experimental protocol and experimental method to illustrate the heterogeneous properties of mudstone and the necessity of the targeting nanoindentation technique (Sect. 2). A theoretical analysis of nanoindentation creep constitutive models and the Oliver–Pharr method followed; the creep models are three viscoelastic models used to fit the nanoindentation strain–time curves (Sect. 3). The calculating and fitting results of nanoindentation experimental data were then given to distinguish the mechanical properties of the two constituents in mudstone as well as to determine and verify suitable nanoindentation creep model (Sect. 4).

2 Material and methodology

2.1 Material

A broken soft mudstone block obtained from a deep underground coal mine was researched in this study. As shown in Fig. 1a, the coal mine named Tongting is located in Anhui province, China. As well, the sampling layer is above the 7# coal strata deposited at the Permian layer, where the stratigraphic column is presented in Fig. 1b.

To quantify the mineralogical constituents of this mudstone sample, the XRD experiment was carried out based on the standards No. SY/T 5163–2018; D8 ADVANCE (Bruker, Germany) was used to conduct this test at the range of 2θ (2-theta) from 10° to 65° with the scanning speed of $2^\circ/\text{min}$. The powder diffraction spectrum is given in Fig. 2a, which shows that the mudstone consisting of 62.57% kaolinite and 37.43% quartz is a two-constituent geomaterial.

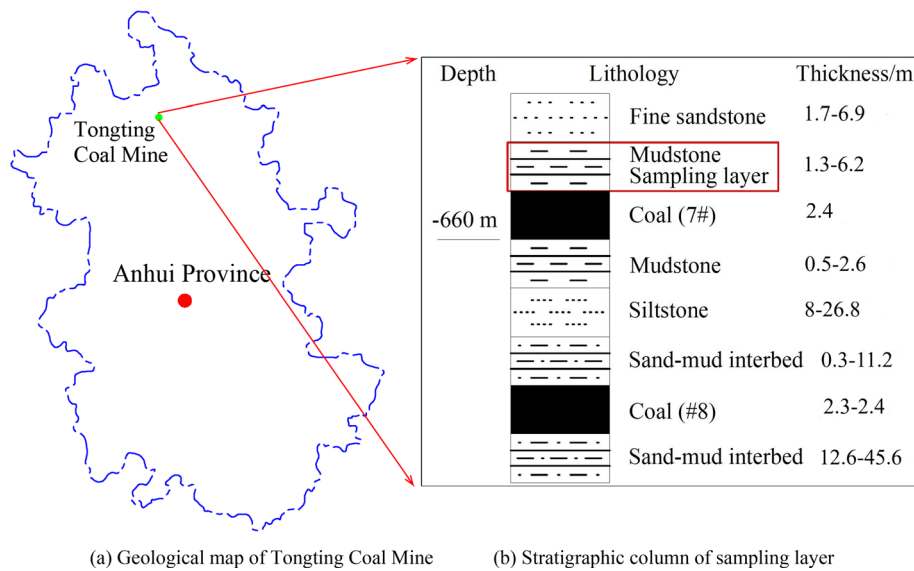
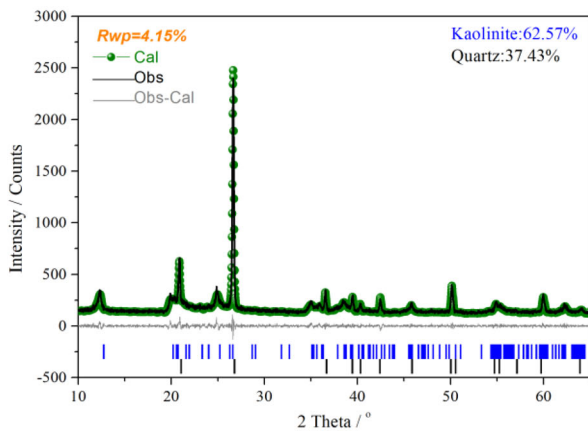
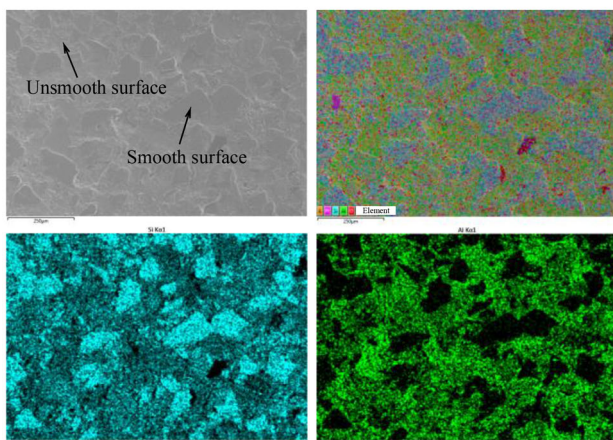


Fig. 1 Sampling area and layer in Anhui Province, China



(a) Powder diffraction spectrum to quantify the mineralogical constituents of mudstone



(b) Images of SEM and EDS for illustrating the distribution of mineralogical constituents in mudstone

Fig. 2 Diffraction spectrum of XRD and images of SEM-EDS

Then, the images of the polished surface of the sample got from SEM-EDS experiments, Fig. 2b to observe and determine the distribution of both constituents in the mudstone sample. The left-top one is the SEM image, in which there are both smooth and unsmooth surfaces; the smooth surfaces are particle-shaped and embedded in the rest unsmooth surfaces regarded as a matrix. The area of unsmooth surfaces is much larger than that of smooth particles, which may represent kaolinite in mudstone and the particles could be quartz. To verify this hypothesis, the right-top EDS image shows the distribution of potassium, silicon, aluminium, and oxygen, and the left-bottom and right-bottom images give the distributions of a single atom of silicon and aluminium, respectively. Since the chemical composition of kaolinite is $Al_2Si_2O_5(OH)_4$ and that of quartz is SiO_2 , the distributions of atoms can help determine the types of minerals in mudstone. The smooth surfaces are the enrichment areas of silicon atom and an oxygen atom, and its enrichment degree of the silicon atom is much higher than the rest areas. Also, the region does not contain aluminium atoms. EDS images verify that on the surface of this mudstone sample, the smooth particles are quartz and the unsmooth surfaces are kaolinite.

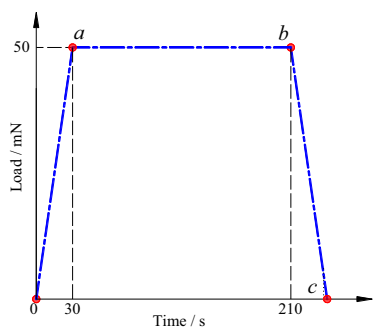
The mudstone is a typical heterogeneous material composed of clay minerals(kaolinite) as matrix and silt inclusions(quartz) embedded in it. The mechanical properties of mudstone are determined by its various constituents (Li et al. 2019b), which encourage us to investigate the mechanical performances of its constituents at the meso-scale. Besides, at the beginning of creep experiments, some standard cylindrical samples (100 mm × Φ50 mm) were prepared to research the mechanical properties of soft mudstone. However, this

experimental plan was dropped due to the influence of macro-scale cracks and pores in the mudstone block on the obtaining of reliable mechanical parameters. Therefore, a new experimental method was used in this study, nanoindentation technique, based on small intact samples.

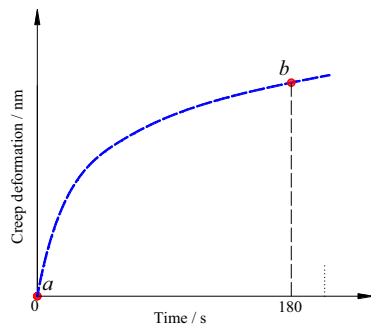
2.2 Methodology

2.2.1 Nanoindentation creep experimental protocol

All nanoindentation creep experiments were conducted using an Anton Paar TTX-NHT³ nano-indentor system equipped with a Berkovich tip. Loads of this system range from 0.1 to 500 mN; the resolutions of load and depth are 20 mN and 0.04 nm, respectively. And the thermal drift of it is less than 0.01 nm/s after allowing thermal equilibrium to be reached for more than 1 h at room temperature (21 °C), which was automatically compensated in this study. As shown in Fig. 3a, a nanoindentation load-time curve is composed of the loading stage (*o-a*), load-holding stage (*a-b*) and unloading stage (*b-c*), where the 180 s load-holding stage at peak load of 50 mN will be used to analyse creep characteristics (Liu et al. 2018). And both the loading and unloading rates are 100 mN/min.



(a) A load-time curve



(b) A creep deformation-time curve

Fig. 3 Nanoindentation creep experimental protocol illustrated by the nanoindentation load-time curve and nanoindentation creep deformation-time curve

After the nanoindentation test, there is a nanoindentation creep deformation-time curve (Fig. 3b). Compared with the deformations during the loading and unloading stages, creep deformation is too small to be observed. Thus, the creep deformation starting from 0 was analysed separately. During the load-holding period, the indenter is displaced further into mudstone. This curve illustrates the portion of displacement that was creep controlled and will be used to analyse the creep characteristics of constituents in mudstone. However, this curve reflects the relationship between creep deformation and time, not that between the typical creep strain and time.

2.2.2 The targeting nanoindentation technique

To make indentations cover representative areas of the material surface and obtain the mechanical properties of all constituents in materials (Slim et al. 2019), the grid nanoindentation method was generally adopted to conduct statistical analysis (Liu et al. 2018). As the name implies, this nanoindentation method has hundreds of indents with uniform intervals on the surfaces of materials of interest to form a grid, which can be used to detect the heterogeneous characteristics of complex materials and perform statistical analysis (Constantinides et al. 2006). Notwithstanding, mechanical parameters obtained from the grid nanoindentation method hinge on the selection of indented surface and the number of indentations (Deirieh et al. 2012; Liu et al. 2018). This experimental method was not of high-efficiency and accuracy. For example, the junction area between mineralogical constituents would affect the accuracy of experimental results.

The whole experimental process used in this study is to replace the grid nanoindentation method, and named as the targeting nanoindentation technique (TNIT) is graphically illustrated in Fig. 4. An intact small mudstone block from a standardized cylindrical sample was cut into a very small volume of mudstone sample (10 mm × 10 mm × 10 mm). The experimental surface fixed with epoxy resin was then polished and exposed. The polishing protocol detailed in (Sun et al. 2020a, b) was followed. This protocol includes a coarse polishing on 3000 grit emery papers and a fine polishing using oil-based diamond suspension with abrasive grain sizes ranging between 3 and 0.5 μm. SEM image shows that there are many meso-scale cracks on the polishing surface. Thus, to measure their creep properties of both constituents in mudstone and avoid the influence of cracks, the intact surfaces including smooth quartz and unsmooth kaolinite were chosen for probing indenter. Images of EDS and SEM illustrate the types and contents of atoms to identify the types of mineralogical ingredients in the meso-scale zone. Finally, nanoindentation experiments will be conducted on both elements in a targeting manner,

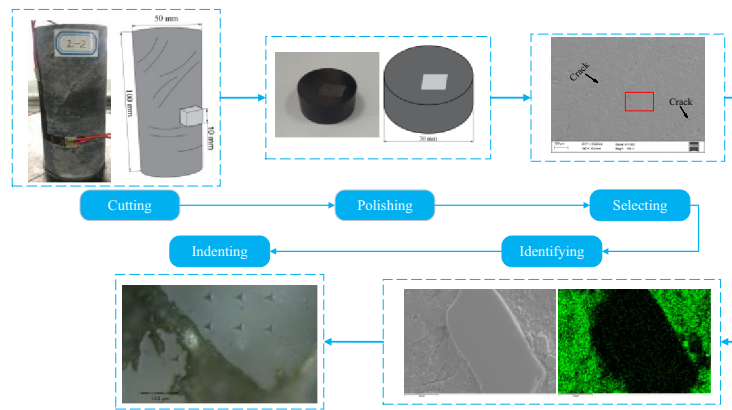


Fig. 4 Process of the targeting nanoindentation technique

and the mechanical properties of both constituents in mudstone can be obtained easily.

The TNIT is a coupled experimental method, where the nanoindentation method is joined with other microstructure/constituent characterization technique. The constituents of mudstone are required to be observed and identified before conducting nanoindentation experiments. During the detecting process, not only the mineralogical constituents are determined, but also the scale separation ($h_{max} < D/10$, where h_{max} is the maximum depth of indenter and D is the size of quartz) is satisfied. The size of quartz is larger than $25 \mu\text{m}$, and that of clay matrix (kaolinite) is larger than quartz in Figs. 2b and 4, while the depth of indents on quartz and kaolinite are around 0.7 and $2.5 \mu\text{m}$. Consequently, the technique can be readily incorporated into an inner computer program of the nanoindentation system to improve the experimental efficiency of the nanoindentation technique on heterogeneous materials, geomaterials in particular.

3 Theories

3.1 Nanoindentation creep model

3.1.1 Nanoindentation strain–time curve

For nanoindentation creep experiments, the stress and strain rate can be written as (Hackney et al. 2012; Mayo and Nix 1988):

$$\sigma = \frac{\beta F}{h^2(t)} \tag{1}$$

$$\dot{\epsilon} = \frac{dh(t)}{dt} \frac{1}{h(t)} \tag{2}$$

And then the strain can be obtained by integrating Eq. (2):

$$\epsilon = \ln \frac{h(t)}{h(0)} \tag{3}$$

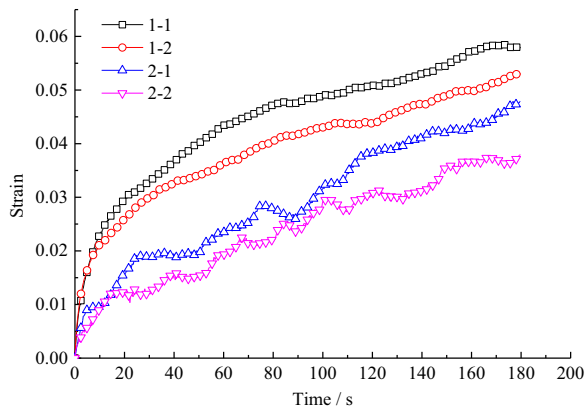
where, σ is the stress, MPa; $\dot{\epsilon}$ is the strain rate, s^{-1} ; ϵ is the strain; $h(t)$ is the indentation depth, nm; t is the creep time, s; $h(0)$ is the indentation depth when creep time is 0, nm; and β is an indenter parameter ($\beta = 0.0407$ for Berkovich indenter (Hackney et al. 2012)).

Based on the nanoindentation creep data obtained from stage *a-b* in Fig. 3, and Eq. (3), four nanoindentation curves of mudstone are shown in Fig. 5. Two curves labeled 1-1 and 1-2 are got from indentations on kaolinite and the other two curves named 2-1 and 2-2 are indented on quartz in mudstone.

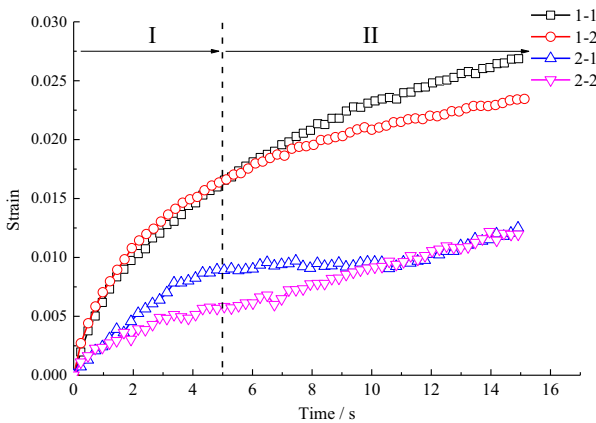
In Fig. 5a, the whole strain–time curves with a load-holding time of 180 s are delivered; and their first stages of 15 s are enlarged in Fig. 5b to help observe the initial part of the load-holding period. The patterns of nanoindentation strain–time curves of both constituents in mudstone are all remarkably similar in form. These curves can be divided into (i) transient creep stage and (ii) steady creep stage. During the period of the transient creep stage, the strain rates are very considerable and decrease sharply with time. After recording the steady stage, the strain develops at almost a constant rate. Also, the load-holding time of 5 s is the dividing point between two stages. Note that there is no tertiary (accelerating) creep stage and initial instantaneous strain in nanoindentation creep-time curves. Consequently, nanoindentation creep curves can be expressed by viscoelastic creep models that do not include elastic elements in series and plastic elements.

3.1.2 Nanoindentation viscoelastic creep models

Here, based on the patterns of nanoindentation strain–time curves, three nanoindentation viscoelastic creep models were proposed in Fig. 6.



(a) Strain-time curves with the load-holding time of 180 s



(b) Strain-time curves with the initial load-holding time of 15 s

Fig. 5 Nanoindentation strain–time curves of kaolinite (1-1 and 1-2) and quartz (2-1 and 2-2) in mudstone

For the elastic element in Fig. 6, the stress (σ) is proportional to the strain (ε), while for the viscous element, it is proportional to the strain rate ($\dot{\varepsilon}$ or $d\varepsilon/dt$). The relationship between stress and strain can be written as Eq. (4) for the elastic element; and that between stress and strain rate, for the viscous element is given in Eq. (5).

$$\sigma = E\varepsilon \tag{4}$$

$$\sigma = \eta\dot{\varepsilon} = \eta \frac{d\varepsilon}{dt} \tag{5}$$

where, E is the modulus, GPa, and η is the viscosity, GPa s.

According to the stress and strain relationship of the parallel and the series structures in Fig. 6, the creep function of the Kelvin model can be summarized as:

$$\varepsilon = \frac{\sigma}{E_1} \left(1 - e^{-\frac{E_1 t}{\eta_1}} \right) \tag{6}$$

The standard viscoelastic model and the extended viscoelastic model can be collected by:

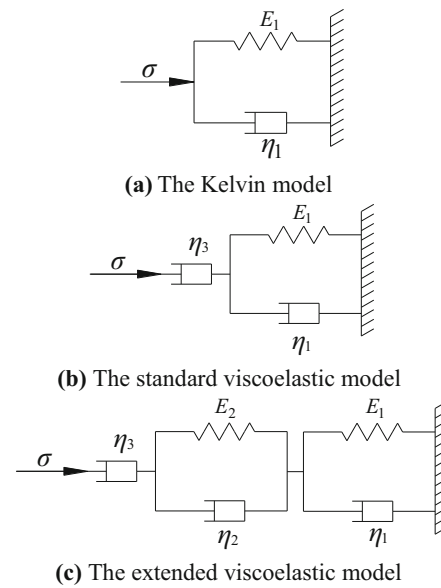


Fig. 6 Three nanoindentation creep models. *Notes* **a** The Kelvin model, with one elastic element and one viscous element in parallel; **b** the standard viscoelastic model, with one viscous element and one Kelvin model in series; and **c** the extended viscoelastic model, with one viscous element and two Kelvin models in series

$$\varepsilon = \sum_{i=1}^n \frac{\sigma}{E_i} \left(1 - e^{-\frac{E_i t}{\eta_i}} \right) + \frac{\sigma}{E_{n+1}} t \tag{7}$$

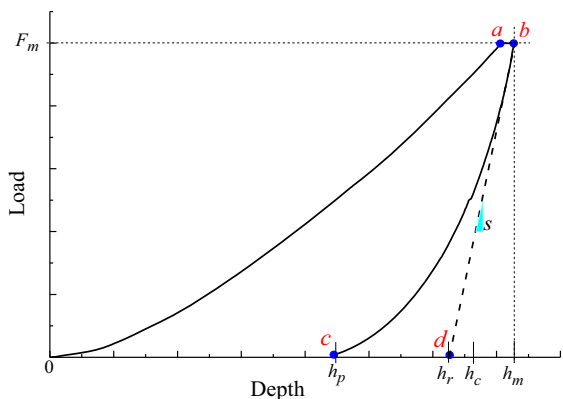
where, n is the number of the Kelvin model in series in a creep viscoelastic model. If $n = 1$, Eq. (7) is the standard viscoelastic model; and if $n \geq 2$, it is the extended viscoelastic model. For fitting the nanoindentation creep strain–time curves, Eq. (7) is further simplified as:

$$\varepsilon = \sum_{i=1}^n A_i (1 - e^{-B_i t}) + Ct \tag{8}$$

where, A_i , B_i and C are fitting constants, and $A_i = \sigma/E_i$, $B_i = E_i/\eta_i$ and $C = \sigma/E_{n+1}$.

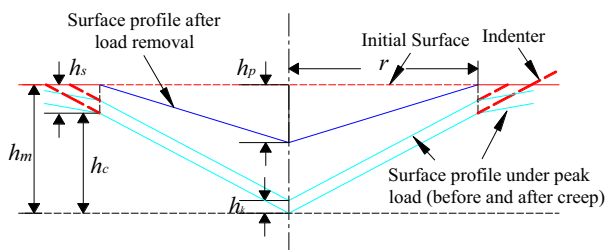
3.2 Oliver-Pharr method

The Oliver-Pharr method gives the hardness and elastic modulus of materials by accounting for the curvature in the unloading stage of the load-depth curve and indentation profile (Oliver and Pharr 1992, 2004). As shown in Fig. 7a, a typical load-depth curve can be obtained as the indenter enters into and exits from the surface of mudstone. The curve consists of a loading segment ($o-a$), load-holding segment ($a-b$), and unloading segment ($b-c$); also, segment $b-d$ is the curve tangent of unloading segment at its initial portion. In Fig. 7b, a typical Berkovich indentation is composited by two surface profiles under load (before and after the load-holding segment or creep) and the residual surface profile after load removal.



(a) A load-depth curve from a typical indentation test

Notes: F_m is the peak load exerted by the indenter, mN; h_m is the maximum depth of indentation, nm; h_c is the contact depth of indentation under the peak load F_m , nm; h_p is the plastic indentation depth after complete unloading, nm; h_r is the tangent depth of unloading curve, nm; S is the contact stiffness, mN/nm.



(b) An indentation profile including initial surface, residual surface and surfaces before and after creep deformation

Notes: h_s is the sinking depth due to load, nm, where $h_s = h_m - h_c$; h_k is the creep depth caused by the load-holding segment (b), nm.

Fig. 7 Nanoindentation calculating schematic diagram of Oliver-Pharr method

It is noted that the load-holding method is mandatory to derive stable unloading data for the calculation of hardness and elastic modulus (Hu and Li 2015; Shi et al. 2019; Zeng et al. 2019) and the holding time is 180 s in this study (Liu et al. 2018). The stable unloading curve is usually well described by a simple power relation (Oliver and Pharr 1992):

$$F = \alpha(h - h_p)^m \tag{9}$$

where, α and m are the power law fitting constants and determined by fitting procedure. Then the contact stiffness is calculated by analytically differentiating this expression at the peak load or the maximum depth, i.e.,

$$S = \left(\frac{dF}{dh} \right)_{F=F_m/h=h_m} = \alpha m(h_m - h_p)^{m-1} \tag{10}$$

The contact depth h_c and the projected area of contact between the indenter and indented constituents A_c are measured by:

$$h_c = h_m - \varepsilon(h_m - h_r), \tag{11}$$

$$A_c = 24.5h_c^2 + C_1h_c^4 + C_2h_c^{1/2} + \dots + C_8h_c^{1/128} \tag{12}$$

where, C_1, \dots, C_8 are the fitting constants; ε is the geometric constant for Berkovich indenter ($\varepsilon = 0.75$ (Oliver and Pharr 1992)); A_c is the projected contact area at peak load, nm². Note that the lead term of Eq. (12) describes Berkovich indenter perfectly.

As a result, the hardness is the average load under the indenter tip and reduced modulus can be calculated from BASH formula (Bulychev et al. 1975).

$$H_{IT} = \frac{F_m}{A_c} \tag{13}$$

$$E_r = \frac{S\sqrt{\pi}}{2\eta\sqrt{A_c}} \tag{14}$$

where, H_{IT} is the hardness, MPa; E_r is the reduced modulus, GPa; η is the geometric constant for Berkovich indenter ($\eta = 1.034$ (Oliver and Pharr 2004)). When the effects of non-rigid indenters on the measurement of elastic modulus of mudstone are ignored, reduced modulus can be used to represent it. Otherwise, it can be calculated by

$$\frac{1 - \nu_{IT}^2}{E_{IT}} = \frac{1}{E_r} - \frac{1 - \nu_i^2}{E_i} \tag{15}$$

where, ν_{IT} is the general Poisson's ratio of constituents in mudstone and $\nu_{IT} = 0.3$ in this study; E_i and ν_i are the elastic modulus and the Poisson's ratio of the diamond indenter and $E_i = 1141$ GPa and $\nu_i = 0.07$ (Oliver and Pharr 1992, 2004).

4 Results and discussions

4.1 Hardness and elastic modulus of kaolinite and quartz

Two nanoindentation tests were made on two constituents (kaolinite and quartz) in mudstone to calculate their hardness and elastic modulus. In Fig. 8, the nanoindentation load-time curves and indentations on kaolinite are labelled 1-1 and 1-2; and the results of quartz are named 2-1 and 2-2.

The load-depth curves on different constituents have the same pattern: During the loading segment, the depths increase sharply with the load at first and then slightly;

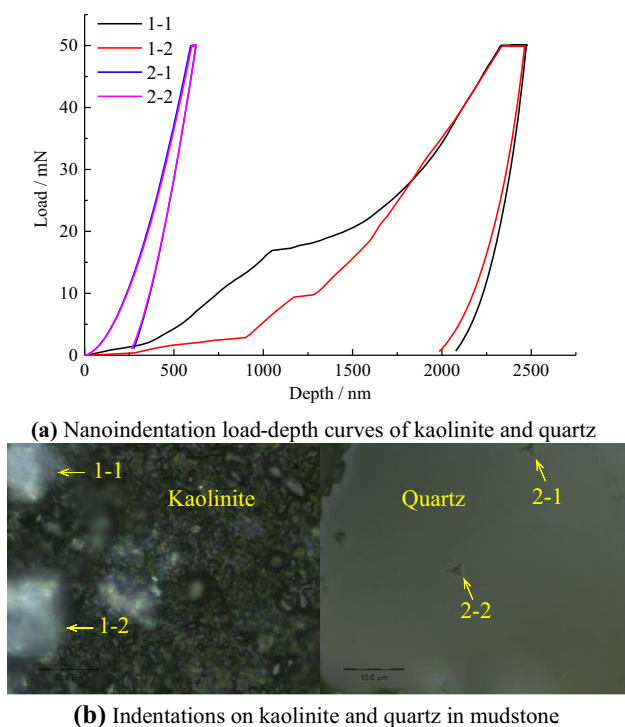


Fig. 8 Load-depth curves of two constituents in mudstone

there is a small creep deformation during the load-holding segment; and after unloading, elastic deformations recover while there are unrecoverable plastic deformations. However, for different constituents, the magnitudes of depths are not the same. The responses associated with the indentations on kaolinite (1-1 and 1-2) give deeper indentation maximum depth (Approx. 2500 nm); while the responses associated with an indentation in quartz have lower indentation maximum depths (Approx. 700 nm).

Based on the typical Oliver-Pharr method, the hardness and elastic modulus were calculated to distinguish the mineralogical constituents. In Table 1, the mean values of hardness and elastic modulus of kaolinite are 355.75 MPa and 17.79 GPa, respectively. And that of quartz in the mudstone are much greater than them, which are

Table 1 Hardness and elastic modulus of kaolinite and quartz in mudstone

Sample	E_{IT} (GPa)	H_{IT} (MPa)
1-1	18.76	352.51
1-2	16.81	358.98
Mean values	17.79	355.75
2-1	67.08	8953.40
2-2	66.00	9157.80
Mean values	66.54	9055.60

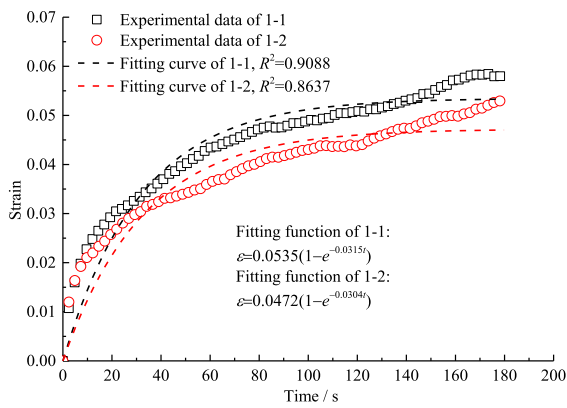
9055.60 MPa and 66.54 GPa. According to prior studying results, the median values for hardness and elastic modulus of sand grain are 10.74 GPa and 66.9 GPa, respectively (Daphalapurkar et al. 2010); and that of Cluster 1 (organic matter or clays) of shales labeled Sample 2, Sample 3 and Sample 4 are from 16.36 to 18.57 GPa (Li et al. 2019a), which verifies the accuracy obtained in this study. The mechanical performances of the kaolinite matrix are much smaller than that of quartz in mudstone, which explains why the argillaceous rocks are soft. For one constituent, the calculated mechanical parameters are close, meaning the targeting nanoindentation technique can be used to obtain the mechanical parameters of various mineralogical compositions in this mudstone.

4.2 Nanoindentation creep parameters

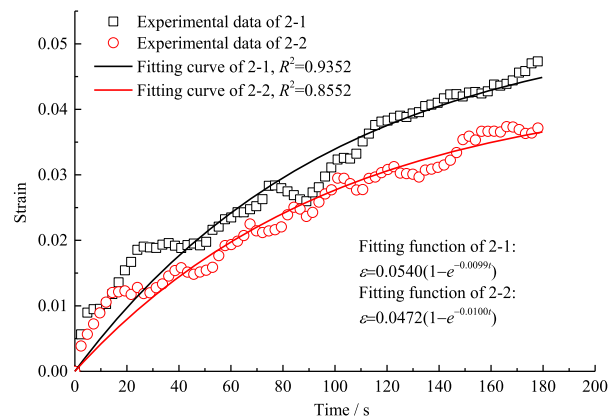
In this section, the proposed nanoindentation creep viscoelastic models in Fig. 6, will be used to fit the nanoindentation experimental data on kaolinite and quartz in mudstone. Figure 9 gives the fitting results of kaolinite by using the Kelvin model, the standard viscoelastic model, and the extended viscoelastic model, respectively. Figure 10 shows that of quartz in mudstone.

Fitting curves by using the Kelvin model did not generate desirable results. As shown in Figs. 9a and 10a, the Kelvin model cannot fit the transient creep stage, where both kaolinite and quartz in mudstone have high strain rates. When describing the final part of the steady creep stage by the Kelvin model, the strain rate is zero, which brings a decided contrarian view to the steady creep stage of nanoindentation creep strain–time curves. Consequently, the Kelvin model cannot be used to describe the creep properties of constituents in mudstone. The values of R^2 less than 0.94 also show that the fitting goodness of the Kelvin model is much weaker than the other two viscoelastic models.

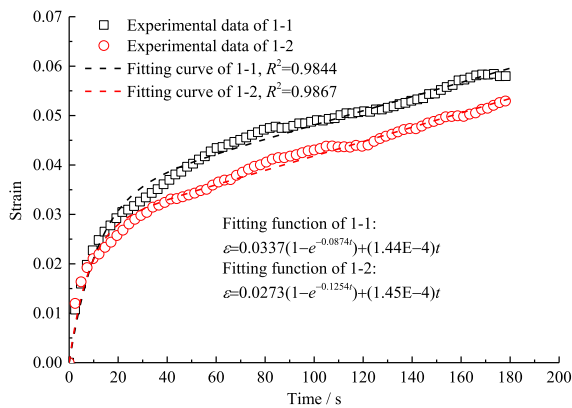
For the viscoelastic models consisting of a viscous element and one or several Kelvin models, fitting results are very good. This result shows that the creep model presented by Eq. (8) can be used to describe the nanoindentation creep behaviors of both constituents in mudstone and the more of the number of the Kelvin models, the better of the fitting results. However, with the increase of the number of the Kelvin models, the fitting constants are probably fallacious. For example, as shown in Fig. 10c, the coefficient of the first-order term of 2-2 is -3.24×10^{-4} , which should be a positive value in reality; and the fitting value of E_2/η_2 for experiment labeled 2-1 is much larger than that of the experiment 2-2. Consequently, for calculating the creep parameters, the standard viscoelastic model is the most useful model among them.



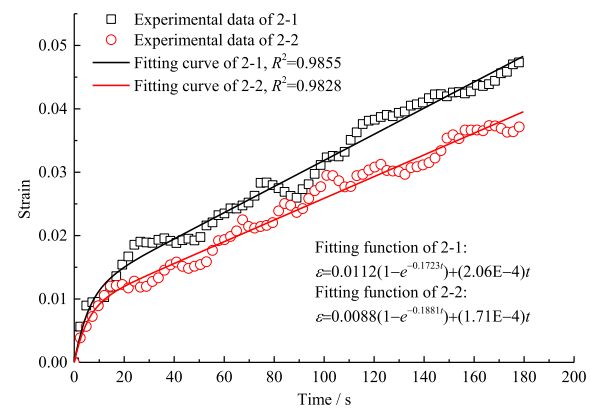
(a) The Kelvin model



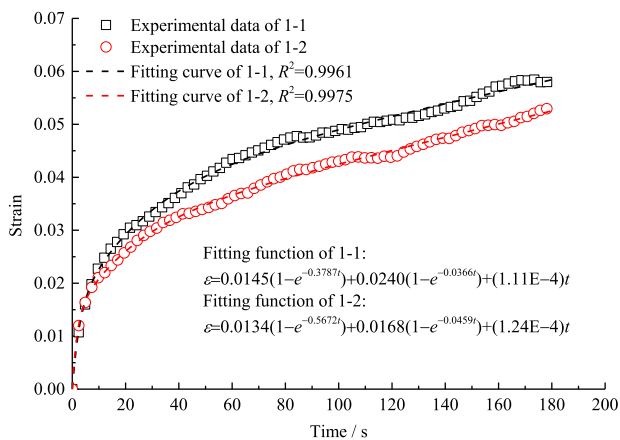
(a) The Kelvin model



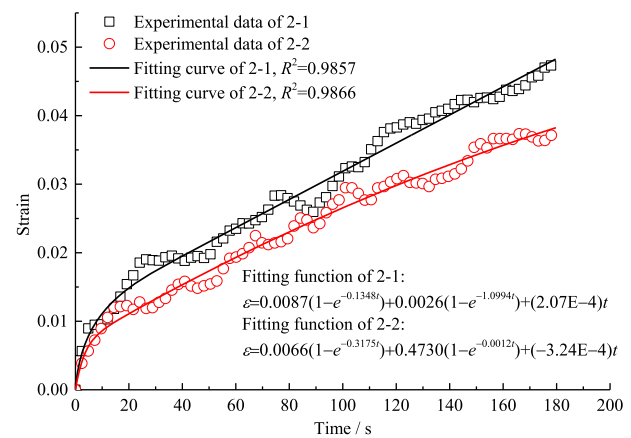
(b) The standard viscoelastic model



(b) The standard viscoelastic model



(c) The extended viscoelastic model



(c) The extended viscoelastic model

Fig. 9 Fitting results of kaolinite by using the Kelvin model, the standard viscoelastic model, and the extended viscoelastic model

According to the fitting results by using the standard viscoelastic model, the creep parameters of both kaolinite and quartz in mudstone can be obtained, as shown in Table 2.

Fig. 10 Fitting results of quartz by using the Kelvin model, the standard viscoelastic model, and the extended viscoelastic model

Note that the values of h_0 was got from the mean values during the load-holding period to minimize the influence of creep deformations on calculated results. And concurring with the above-calculated hardness and elastic modulus, the creep parameters of different constituents in the

Table 2 Creep parameters of kaolinite and quartz in mudstone

Sample	h_0 (nm)	σ (MPa)	A_1	B_1 (GPa s)	C (10^{-4} GPa s)	E_1 (GPa)	η_1 (GPa s)	η_2 (GPa s)
1-1	2402.35	353.07	0.0337	− 0.0874	1.44	10.48	119.87	2451.88
1-2	2398.59	353.19	0.0273	− 0.1254	1.45	12.94	103.17	2435.79
					Mean values	11.71	111.52	2443.83
2-1	607.66	5503.47	0.0112	− 0.1723	2.06	491.38	2851.89	26,715.89
2-2	612.24	5430.20	0.0088	− 0.1881	1.71	617.07	3280.54	31,755.58
					Mean values	554.23	3066.21	29,235.73

mudstone are various, too. For example, the mean value of the first viscous element of kaolinite is 111.52 GPa s, while this value of quartz is much larger, which is 3066.21 GPa s. This comparison means that the soft clay minerals in mudstone have large creep deformation, which reveals the mechanism of large creep deformation of argillaceous engineering.

4.3 Verification of nanoindentation creep model

To verify that the viscoelastic creep models (Eq. (8)) can perfectly fit the nanoindentation strain–time curves and that the calculated creep parameters may be unreliable when $n \geq 2$, four nanoindentation experiments were made on the quartz in a sandstone obtain from Suntuan Coal Mine, Anhui, China. Figure 11 gives the load–depth curves and indentations of them. The load–depth curves were used to calculate the elastic modulus and hardness and analyse the creep characteristic of quartz in sandstone; the indentations illustrate the application of the targeting nanoindentation technique.

Using the standard viscoelastic model and the extended viscoelastic model to fit the four nanoindentation strain–time curves of quartz in sandstone, fitting results are shown in Fig. 12. And the fitting constants are given in Table 3.

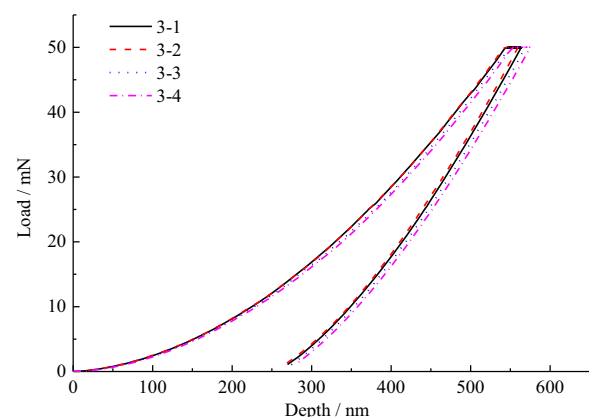
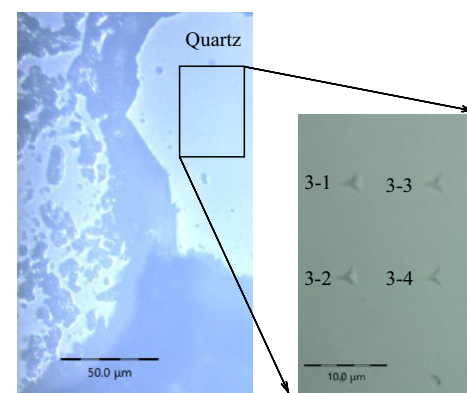
According to the fitting results in Fig. 12, both the standard viscoelastic model and the extended viscoelastic model can perfectly fit the nanoindentation data, with goodness above 0.99. However, like the obtained results in Sect. 4.2, fitting constants derived from the extended viscoelastic model tend to be mutually contradictory in Table 3, which are bold in this table.

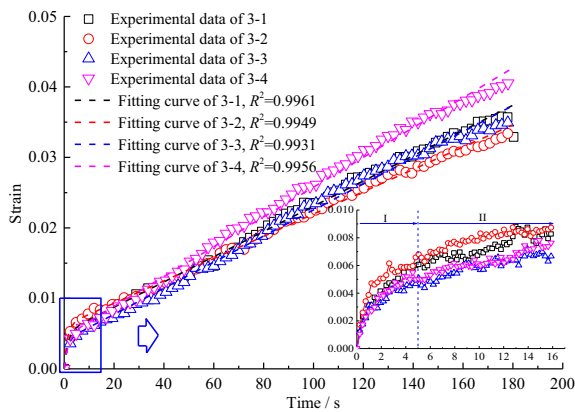
As a result, the standard viscoelastic model was verified to be a suitable function to fit nanoindentation creep strain–time curves and calculate the creep parameters. The obtained hardness, elastic modulus, and creep parameters are shown in Table 4. It also shows that the mechanical properties of quartz in sandstone are slightly larger than that of quartz in mudstone. For example, the mean elastic modulus of quartz in sandstone is 85.81 GPa, and that in mudstone is 66.54 GPa. The reason for the smaller mechanical properties of quartz in mudstone is probably

due to the influence of soft kaolinite as a matrix in mudstone or the crystal orientation since quartz is highly anisotropic (Eliyahu et al. 2015; Timms et al. 2010).

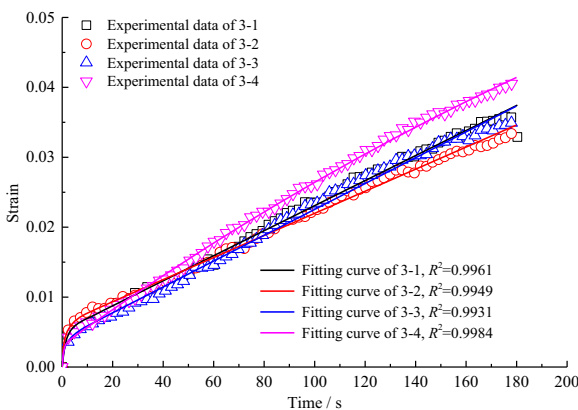
5 Conclusions

In this paper, the viscoelastic characteristics of kaolinite and quartz in mudstone were investigated by using the targeting nanoindentation technique. Conclusions are as follows.

**(a)** Four load–depth curves on quartz in sandstone**(b)** Four indentations on quartz in sandstone**Fig. 11** Four load–depth curves and indentations on quartz in sandstone



(a) The standard viscoelastic model



(b) The extended viscoelastic model

Fig. 12 Fitting results of strain–time curves of quartz in sandstone by using the standard viscoelastic model and the extended viscoelastic model

- (1) The examined soft mudstone sample in this study is composed of kaolinite and quartz, in which kaolinite is soft, as well as a matrix with hard quartz embedded in it.
- (2) For broken soft rocks that cannot provide intact standardized samples, the nanoindentation method can be used to investigate their mechanical

Table 4 Mechanical parameters of quartz in sandstone

Sample	H_{IT} (MPa)	E_{IT} (GPa)	E_1 (GPa)	η_1 (GPa s)	η_2 (GPa s)
3-1	10,416.00	86.55	1280.81	1884.09	37,207.76
3-2	10,440.00	87.99	1083.67	1364.14	42,523.90
3-3	10,078.00	85.38	1629.51	2010.00	35,232.55
3-4	9912.00	83.32	1394.21	2331.46	30,395.20
Mean values	10,211.50	85.81	1347.05	1897.42	36,339.85

properties by yielding stable mechanical parameters. Compared with the grid nanoindentation technique, the TNIT is efficient. This experimental technique can be realized by coupling the nanoindentation technique and observing experimental methods, like XRD, SEM, and EDS. Using this experimental method, the mechanical properties of constituents in geomaterials can be quickly obtained.

- (3) The nanoindentation creep strain–time curve reflects the viscoelastic properties of mudstone. This curve can be divided into two stages: a transient stage and a steady stage. The standard viscoelastic model consisting of a viscous element where a Kelvin model in series can perfectly fit the nanoindentation creep strain–time curves of mudstone and provide reasonable rheological parameters. And the proposed model was also used to fit creep curves of quartz in sandstone with high goodness, which verifies the nanoindentation creep model. Even though the extended viscoelastic can better fitting nanoindentation creep curves, it could yield unreasonable creep parameters.
- (4) The mechanical properties of quartz in mudstone and sandstone are slightly different, which may be due to the influence of soft clay minerals in mudstone that softens the mechanical performance of quartz in it or the crystal orientation of quartz.

Table 3 Mechanical parameters of quartz in sandstone

Sample	The standard viscoelastic model			The extended viscoelastic model				
	A_1	B_1 (GPa s)	C (10^{-4} GPa s)	A_1	B_1 (GPa s)	A_2 (GPa s)	B_2 (GPa s)	C (10^{-4} GPa s)
3-1	0.0052	– 0.6798	1.79	0.0026	– 0.6793	0.0026	– 0.6803	+ 1.79
3-2	0.0062	– 0.7944	1.58	0.0029	– 2.6268	0.0033	– 0.4183	+ 1.58
3-3	0.0040	– 0.8107	1.85	0.0019	– 2.7350	0.0022	– 0.4208	+ 1.85
3-4	0.0046	– 0.5980	2.11	0.0031	– 1.6863	0.5569	+ 9.9586	– 2.95

Acknowledgements The work presented in this paper was supported by the projects of “the Fundamental Research Funds for the Central Universities (2020ZDPY0221)” and “the Guizhou Science and Technology Department ([2020]2Y026)”. The authors are also grateful to the anonymous reviewers for carefully reading the manuscript and providing many helpful comments. Sun Changlun acknowledges, in particular, the powerful support received from his wife, Zhou Fan, over the years.

Open Access This article is licensed under a Creative Commons Attribution 4.0 International License, which permits use, sharing, adaptation, distribution and reproduction in any medium or format, as long as you give appropriate credit to the original author(s) and the source, provide a link to the Creative Commons licence, and indicate if changes were made. The images or other third party material in this article are included in the article’s Creative Commons licence, unless indicated otherwise in a credit line to the material. If material is not included in the article’s Creative Commons licence and your intended use is not permitted by statutory regulation or exceeds the permitted use, you will need to obtain permission directly from the copyright holder. To view a copy of this licence, visit <http://creativecommons.org/licenses/by/4.0/>.

References

- Abedi S, Slim M, Hofmann R, Bryndzia T, Ulm F-J (2016) Nanochemo-mechanical signature of organic-rich shales: a coupled indentation–EDX analysis. *Acta Geotech* 11(3):559–572
- Alstadt KN, Katti KS, Katti DR (2015) Nanoscale morphology of kerogen and in situ nanomechanical properties of green river oil shale. *J Nanomech Micromech* 6(1):04015003
- Auvray C, Lafrance N, Bartier D (2017) Elastic modulus of claystone evaluated by nano-/micro-indentation tests and meso-compression tests. *J Rock Mech Geotech Eng* 9(1):84–91
- Bulychev S, Alekhin V, Shorshorov M, Ternovskii A, Shnyrev G (1975) Determining Young’s modulus from the indenter penetration diagram. *Indus Lab* 41(9):1409–1412
- Constantinides G, Ravi Chandran K, Ulm F, Van Vliet K (2006) Grid indentation analysis of composite microstructure and mechanics: principles and validation. *Mat Sci Eng A-Struct* 430(1–2):189–202
- Danesh NN, Chen ZW, Aminossadati SM, Kizil MS, Pan ZJ, Connell LD (2016) Impact of creep on the evolution of coal permeability and gas drainage performance. *J Nat Gas Sci Eng* 33:469–482
- Danesh NN, Chen ZW, Connell LD, Kizil MS, Pan ZJ, Aminossadati SM (2017) Characterisation of creep in coal and its impact on permeability: an experimental study. *Int J Coal Geol* 173:200–211
- Daphalapurkar N, Wang F, Fu B, Lu H, Komanduri R (2010) Determination of Mechanical Properties of Sand Grains by Nanoindentation. *Exp Mech* 5(5):719–728
- Deirieh A, Ortega J, Ulm F, Abousleiman Y (2012) Nanochemomechanical assessment of shale: a coupled WDS-indentation analysis. *Acta Geotechnica* 7(4):271–295
- Eliyahu M, Emmanuel S, Day-Stirrat R, Macaulay C (2015) Mechanical properties of organic matter in shales mapped at the nanometer scale. *Mar Petrol Geol* 59:294–304
- Fan Z, Hanqun G, Jianjian Z, Dawei H, Qian S, Jianfu S (2017) Experimental study of micro-mechanical properties of granite. *Chin J Rock Mechan Eng* 36(S2):3864–3872
- Guery AAC, Cormery F, Shao JF, Kondo D (2008) A micromechanical model of elastoplastic and damage behavior of a cohesive geomaterial. *Int J Solids Struct* 45(5):1406–1429
- Guo Z, Wang Q, Yin S, Kuai X, Yan D, Li M, Qu Y (2019) The creep compaction behavior of crushed mudstones under the step loading in underground mining. *Int J Coal Sci Technol* 6(3):408–418
- Guo ZH, Vu PNH, Hussain F (2018) A laboratory study of the effect of creep and fines migration on coal permeability during single-phase flow. *Int J Coal Geol* 200:61–76
- Hackney S, Aifantis K, Tangtrakarn A, Shrivastava S (2012) Using the Kelvin-Voigt model for nanoindentation creep in Sn-C/PVDF nanocomposites. *Mater Sci Tech-Lond* 28(9–10):1161–1166
- He M, Xie H, Peng S, Jiang Y (2005) Study on rock mechanics in deep mining engineering. *Chin J Rock Mechan Eng* 24(16):2803–2813
- Hu C, Li Z (2015) A review on the mechanical properties of cement-based materials measured by nanoindentation. *Constr Build Mater* 90:80–90
- Jia CJ, Xu WY, Wang RB, Wang SS, Lin ZN (2018) Experimental investigation on shear creep properties of undisturbed rock discontinuity in Baihetan hydropower station. *Int J Rock Mech Min* 104:27–33
- Kalei GN (1968) Some results of microhardness test using the depth of impression. *Mashinovedenie* 4(3):105–107
- Kang JH, Zhou FB, Liu C, Liu YK (2015) A fractional non-linear creep model for coal considering damage effect and experimental validation. *Int J Nonlin Mech* 76:20–28
- Kong L, Ostadhassan M, Zamiran S, Liu B, Li C, Marino GG (2019) Geomechanical upscaling methods: comparison and verification via 3D printing. *Energies* 12(3):382
- Li C, Ostadhassan M, Kong L, Bubach B (2019a) Multi-scale assessment of mechanical properties of organic-rich shales: A coupled nanoindentation, deconvolution analysis, and homogenization method. *J Petrol Sci Eng* 174:80–91
- Li G, Sun C, He J, Sun Y, Dong Y, Zhao H (2019b) Macro- and meso-scale simulation study of the strength-weakening property of soft mudstone affected by water. *J China Univ Min Technol* 48(5):935–942
- Li X, Yang C, Ren T, Nie B, Zhao C, Liu S, Jiang T (2017) Creep behaviour and constitutive model of coal filled with gas. *Int J Min Sci Technol* 27(5):847–851
- Liu K, Ostadhassan M, Bubach B (2018) Application of nanoindentation to characterize creep behavior of oil shales. *J Petrol Sci Eng* 167:729–736
- Liu K, Ostadhassan M, Bubach B, Dietrich R, Rasouli V (2017) Nano-dynamic mechanical analysis (nano-DMA) of creep behavior of shales: Bakken case study. *J Mater Sci* 53(6):4417–4432
- Liu ZB, Xie SY, Shao JF, Conil N (2015) Effects of deviatoric stress and structural anisotropy on compressive creep behavior of a clayey rock. *Appl Clay Sci* 114:491–496
- Lu YL, Wang LG (2017) Effect of water and temperature on short-term and creep mechanical behaviors of coal measures mudstone. *Environ Earth Sci* 76(17):597
- Magnenet V, Auvray C, Francius G, Giraud A (2011) Determination of the matrix indentation modulus of Meuse/Haute-Marne argillite. *Appl Clay Sci* 52(3):266–269
- Mayo M, Nix W (1988) A micro-indentation study of superplasticity in Pb, Sn, and Sn-38 wt% Pb. *Acta Metallurgica* 36(8):2183–2192
- Meng J, Niu J, Junkai X, Kan L (2020) Study on mechanical properties and failure mechanisms of coal at the nanometer scale. *Chin J Rock Mechan Eng* 39(1):84–92
- Mishra B, Verma P (2015) Uniaxial and triaxial single and multistage creep tests on coal-measure shale rocks. *Int J Coal Geol* 137:55–65

- Oliver WC, Pharr GM (1992) An improved technique for determining hardness and elastic modulus using load and displacement sensing indentation experiments. *J Mater Res* 7(6):1564–1583
- Oliver WC, Pharr GM (2004) Measurement of hardness and elastic modulus by instrumented indentation: Advances in understanding and refinements to methodology. *J Mater Res* 19(1):3–20
- Sainoki A, Mitri HS (2017) Numerical investigation into pillar failure induced by time-dependent skin degradation. *Int J Min Sci Technol* 27(4):591–597
- Sha ZH, Pu H, Li M, Cao LL, Liu D, Ni HY, Lu JF (2018) Experimental study on the creep characteristics of coal measures sandstone under seepage action. *Processes* 6(8):110
- Shi X, Jiang S, Lu S, He Z, Li D, Wang Z, Xiao D (2019) Investigation of mechanical properties of bedded shale by nanoindentation tests: A case study on Lower Silurian Longmaxi Formation of Youyang area in southeast Chongqing, China. *Petrol Explor Dev+* 46(1):163–172
- Slim M, Abedi S, Bryndzia LT, Ulm F-J (2019) Role of organic matter on nanoscale and microscale creep properties of source rocks. *J Eng Mech* 145(1):04018121
- Sone H, Zoback MD (2014) Time-dependent deformation of shale gas reservoir rocks and its long-term effect on the in situ state of stress. *Int J Rock Mech Min* 69:120–132
- Sun C, Li G, Gomah ME, Xu J, Rong H (2020a) Experimental investigation on the mechanical properties of crushed coal samples based on the nanoindentation technique. *J China Coal Soc* <https://doi.org/10.13225/j.cnki.jccs.2020.0351>
- Sun C, Li G, Zhang S, Xu J, Yang H (2020b) Mechanical and heterogeneous properties of coal and rock quantified and mapped at the microscale. *Appl Sci* 10(1):342
- Sun J (2007) Rock rheological mechanics and its advance in engineering applications. *Chin J Rock Mechan Eng* 26(6):1081–1106
- Sun Q, Zhang X, Yu Y (2013) Creep constitutive model of cemented body used in backfilling mining. *J China Coal Soc* 38(6):994–1000
- Timms N, Healy D, Reyes-Montes J, Collins D, Prior D, Young R (2010) Effects of crystallographic anisotropy on fracture development and acoustic emission in quartz. *J Geophys Res* 115(B7)
- Xiong ZQ, Song CS, Su CD, Wang XL, Wang C, Hao Y (2019) Uniaxial compression creep relaxation and grading of coal samples via tests on the progressive failure characteristics. *Geofluids* 2019:1–13
- Xu P, Yang S, Guofei C (2014) Modified Burgers model of rocks and its experimental verification. *J China Coal Soc* 39(10):1993–2000
- Yang SQ, Xu P, Ranjith PG (2015) Damage model of coal under creep and triaxial compression. *Int J Rock Mech Min* 80:337–345
- Yang Y, Xing L, Zhang Y, Ma D (2015) Analysis of long-time stability of gypsum pillars based on creep tests. *Chin J Rock Mechan Eng* 34(10):2106–2113
- Zeng Q, Wu Y, Liu Y, Zhang G (2019) Determining the microfracture properties of Antrim gas shale by an improved micro-indentation method. *J Nat Gas Sci Eng* 62:224–235
- Zhang F, Guo H, Hu D, Shao J-F (2018) Characterization of the mechanical properties of a claystone by nano-indentation and homogenization. *Acta Geotech* 13(6):1395–1404
- Zhang Y, Lebedev M, Al-Yaseri A, Yu H (2018) Nanoscale rock mechanical property changes in heterogeneous coal after water adsorption. *Fuel* 218:23–32
- Zhang Y, Lebedev M, Al-Yaseri A, Yu H, Xu X, Iglauer S (2018) Characterization of nanoscale rockmechanical properties and microstructures of a Chinese sub-bituminous coal. *J Nat Gas Sci Eng* 52:106–116
- Zhao J, Zhang D, Wu T, Tang H, Xuan Q, Jiang Z, Dai C (2019) Multiscale approach for mechanical characterization of organic-rich shale and its application. *Int J Geomech* 19(1):04018180
- Zhou HW, Wang LJ, Rong TL, Zhang L, Ren WG, Su T (2019) Creep-based permeability evolution in deep coal under unloading confining pressure. *J Nat Gas Sci Eng* 65:185–196